NANO LETTERS

Coherent Spin Precession and Lifetime-Limited Spin Dephasing in $CsPbBr_3$ Perovskite Nanocrystals

Matthew J. Crane,[‖] Laura M. Jacoby,[‖] Theodore A. Cohen, Yunping Huang, Christine K. Luscombe, and Daniel R. Gamelin*

Cite This: *Nano Lett.* 2020, 20, 8626−8633

ABSTRACT: Carrier spins in semiconductor nanocrystals are promising candidates for quantum information processing. Using a combination of time-resolved Faraday rotation and photoluminescence spectroscopies, we demonstrate optical spin polarization and coherent spin precession in colloidal $CsPbBr_3$ nanocrystals that persists up to room temperature. By suppressing the influence of inhomogeneous hyperfine fields with a small applied magnetic field, we demonstrate inhomogeneous hole transverse spin-dephasing times (T_2^*) that approach the nanocrystal photoluminescence lifetime, such that nearly all emitted photons derive from coherent hole spins. Thermally activated LO phonons drive additional spin dephasing at elevated temperatures, but coherent spin precession is still observed at room temperature. These data reveal several major distinctions between spins in nanocrystalline and bulk $CsPbBr_3$ and open the door for using metal-halide perovskite nanocrystals in spin-based quantum technologies.

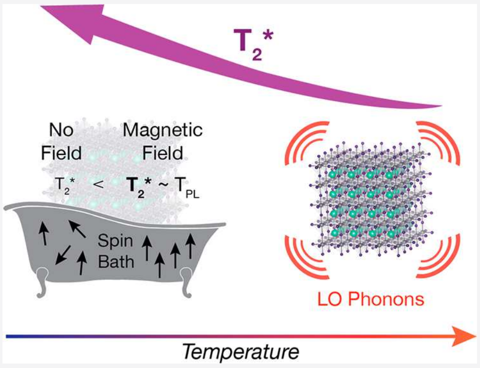

KEYWORDS: *perovskite nanocrystal, spin dephasing, T_2*, time-resolved Faraday rotation, spintronics, quantum information*

Lead-halide perovskites are a promising class of materials with broad potential for optoelectronic applications stemming from their high photoluminescence quantum yields (PLQYs), chemically tunable band gap, large absorption coefficients, and long carrier lifetimes.[1−6] They have also recently emerged as intriguing materials for future spintronic and quantum information applications due to their long spin lifetimes,[7,8] strong spin−orbit coupling,[9] photoinduced spin polarization,[10,11] Rashba effects,[12−14] and long optical coherence.[15,16] Lead-halide perovskites offer the potential for optical generation, manipulation, and read-out of spins[17] and have been proposed as promising candidates for applications such as spin field-effect transistors and single-photon emitters.[7,16,18,19]

Recently, Utzat et al. demonstrated that $CsPbBr_3$ nanocrystals exhibit long optical coherence times, $T_{2,o}$, making them promising single-photon emitters.[16] A valuable figure of merit for single-photon emitters is the percentage of emitted photons that are optically coherent, which approaches 100% when $T_{2,o}$ reaches twice the PL lifetime, τ_{PL}. In $CsPbBr_3$ nanocrystals, Rashba splitting creates a bright lowest excitonic state,[14] enabling fast radiative recombination at low temperatures and a $T_{2,o}/2\tau_{PL}$ ratio up to ∼0.1, comparable to that of diamond color centers[16,20,21] and rivaling those of III−V epitaxial quantum dots.[22] Many other potential quantum-information capabilities, such as spin qubits, emerge in materials with long *spin* lifetimes and appropriate spectroscopic properties to allow all-optical spin generation, manipulation, and read-out.[23,24] For example, some large-scale quantum-information schemes require quantum repeaters or spin-photon interfaces comprising single-photon emitters with long inhomogeneous transverse spin-dephasing times, T_2^*.[25−28] Thus, the combination of promising spin and optical properties could make perovskite nanocrystals attractive for future quantum technologies.

Despite its importance, spin dephasing in lead-halide perovskites has only been investigated in bulk samples,[7,8] and these do not show the long optical coherence times or high PLQYs seen in nanocrystals. Additionally, studies of macroscopic samples do not address possibilities such as confinement-modified exchange interactions and exciton-binding energies,[29,30] size-dependent Rashba effects,[31] modified phonon dispersion, and surface interactions,[32] all of which are critical determinants of spin dynamics in nanocrystals.[33] To date, spin dynamics in metal-halide perovskite nanocrystals have been investigated exclusively using zero-field circularly polarized transient-absorption spectroscopy.[9,11] This technique measures longitudinal spin-flip dynamics, i.e., zero-field T_1, whereas spin *dephasing* (T_2 or T_2^*) is the property of most

Received: August 14, 2020
Revised: November 18, 2020
Published: November 25, 2020

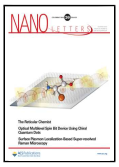

https://dx.doi.org/10.1021/acs.nanolett.0c03329

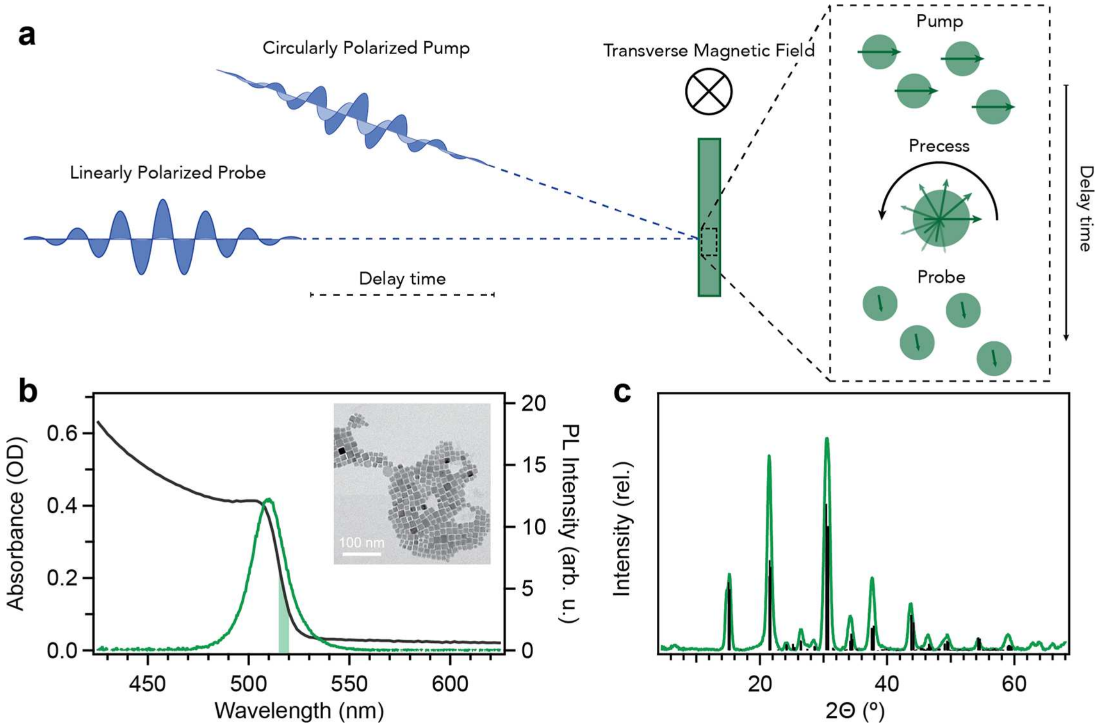

Figure 1. Time-resolved Faraday rotation (TRFR) experiment and $CsPbBr_3$ nanocrystal characterization. (a) Schematic summary of the TRFR experiment, illustrating optical generation of oriented spins in an ensemble of $CsPbBr_3$ nanocrystals using a circularly polarized femtosecond pump pulse resonant with band-edge absorption. The sample resides in a transverse magnetic field, causing the photogenerated spins to precess. A time-delayed linearly polarized probe pulse reads out the ensemble spin projection as a function of delay time, capturing spin-precession and dephasing dynamics. The panel on the right details the microscopic TRFR process for a single pump−probe cycle, highlighting the optical spin generation, spin precession, and read-out via Faraday rotation of the linearly polarized probe. (b) Room-temperature absorption and PL spectra of $CsPbBr_3$ nanocrystals embedded in a thin polymer film (see the SI). The shaded green region illustrates the pump and probe energies used in the TRFR measurements. The inset shows representative TEM images of the $CsPbBr_3$ nanocrystals without polymer. (c) Room-temperature XRD data for the $CsPbBr_3$ nanocrystals examined here. Black sticks illustrate reference reflections for orthorhombic $CsPbBr_3$. For variable-temperature spectroscopic measurements described in the main text, these $CsPbBr_3$ nanocrystals were embedded in films of zwitterion-functionalized fluoropolymer (ZFP3)[37] on c-plane sapphire that showed negligible photon scattering (see the SI for details). The TRFR measurement is extremely sensitive to the polarization of the probe pulse, and scattering scrambles this polarization information.

interest for quantum applications. More detailed investigations of spins in lead-halide perovskite nanocrystals are thus needed.

Here, we use time-resolved Faraday rotation (TRFR) spectroscopy to probe spin-dephasing dynamics in $CsPbBr_3$ nanocrystals for the first time. We observe optical spin polarization and coherent precession of photogenerated holes and identify two distinct dephasing regimes. At low temperatures, spin dephasing is driven by inhomogeneous hyperfine fields and can be suppressed by small magnetic fields, ultimately allowing detection of ensemble hole spin dephasing that is limited primarily by radiative carrier recombination. Exciton−phonon coupling drives spin dephasing at elevated temperatures, but spin coherence is still observed at room temperature in these nanocrystals, in contrast with bulk $CsPbBr_3$.[7,8] The combination of short radiative lifetimes, long optical coherence times, and, now, long spin coherence times highlights the promise of $CsPbBr_3$ nanocrystals for spin-based quantum applications.

Figure 1a illustrates the one-color TRFR experiment used here.[17,34−36] A resonant circularly polarized femtosecond pump pulse generates a polarized excited-state spin population that precesses in a transverse magnetic field and dephases. TRFR probes the ensemble spin projection at different delay times via Faraday rotation of a linearly polarized probe pulse. This experiment yields the inhomogeneous transverse spin-dephasing time, T_2^*, which provides a lower limit for the homogeneous spin coherence time, T_2.

Figure 1b shows room-temperature absorption and PL spectra of a representative $CsPbBr_3$ nanocrystal thin film used in these TRFR experiments. From TEM (Figure 1b, inset), these nanocrystals have edge lengths of 10 ± 2 nm, slightly larger than the Bohr exciton diameter of ∼7 nm.[3] The sample shows bright room-temperature PL at 2.43 eV that is slightly Stokes shifted from the first excitonic absorption maximum (2.45 eV), with a room-temperature PLQY of ∼30% under the TRFR conditions used here. Figure 1c plots X-ray diffraction (XRD) data collected for these nanocrystals, showing reflections consistent with the orthorhombic perovskite structure.

Figure 2a plots 4.5 K TRFR traces collected for these $CsPbBr_3$ nanocrystals at various transverse magnetic fields, B_T, from 0 to 0.60 T. At the highest field, the data show oscillations that decay within ∼600 ps. At lower fields, the oscillation frequency decreases, and at zero field, the trace shows only a nonoscillatory decay. At all nonzero fields, these oscillations can be associated with a single primary frequency, confirmed by the presence of single dominant peaks in the fast-Fourier transforms (FFTs) of these traces (Figure 2b, inset and Figure S7, *vide infra*). These oscillations correspond to the Larmor precession frequencies (ω_L) of the photogenerated

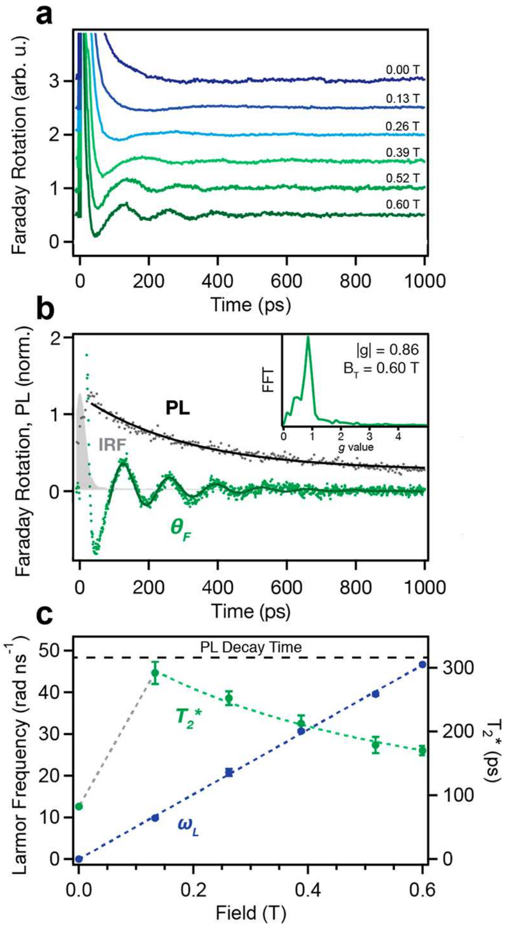

Figure 2. Spin dynamics in $CsPbBr_3$ nanocrystals measured at 4.5 K. (a) TRFR of $CsPbBr_3$ nanocrystals measured at different transverse magnetic field strengths. The oscillation frequency increases with increasing magnetic field. (b) Comparison of the TRFR trace measured at 0.60 T (green) and the PL intensity decay (black) measured under the same conditions (λ_{ex} = 517 nm, T = 4.5 K). The gray curve corresponds to the instrument response function of the PL lifetime measurement. The solid curves show fits of the data. The TRFR trace is fitted with a decaying sinusoidal function, yielding a decay time constant of T_2^* = 170 ps. The PL decay is fitted with a monoexponential function, yielding a decay time constant of τ_{PL} = 312 ± 11 ps. The inset plots the fast Fourier transform (FFT) of the TRFR trace and shows a single dominant resonance at |g| = 0.86. Detailed fits for each trace from panel a are provided as Supporting Information (Figure S8). (c) Dependence of the Larmor frequency, ω_L (blue), and ensemble spin-dephasing time, T_2^* (green), on the transverse magnetic-field strength, B_T. The Larmor frequency increases linearly with increasing magnetic field, and the slope (dashed blue line) gives |g| = 0.88. The initial increase in T_2^* with applied field is attributed to suppression of hyperfine-induced local-field heterogeneity. The decrease in T_2^* at larger applied fields is attributed to g-factor distribution, and the data from 0.13 to 0.60 T are fitted (dashed green line) using eq 2, yielding Δg = 0.07. The gray dashed line between 0 and 0.16 T is a guide to the eye. For comparison, the black horizontal dashed line shows the PL decay time (312 ps) measured at 4.5 K under the same conditions.

spins and are related to the spin's g-value by $\omega_L = g\mu_B B_T/\hbar$, where μ_B is the Bohr magneton. The TRFR amplitudes are proportional to the Faraday rotation angle, θ_F, and reflect the sample's magnetization projected along the optical axis. The oscillations can be fitted with the exponentially decaying oscillatory function given in eq 1.

$$\theta_F(t) = Ae^{-t/T_2^*}\cos(\omega_L t + \phi) \tag{1}$$

Figure 2b shows a representative fit of the B_T = 0.60 T TRFR data with eq 1, which yields $\omega_L \sim 47$ rad ns^{-1} and $T_2^* \sim 170 \pm 7$ ps. Figure 2b also compares the TRFR trace with the 4.5 K time-resolved PL of the same $CsPbBr_3$ nanocrystals measured under identical conditions. The PL decays monoexponentially with a lifetime of τ_{PL} = 312 ± 11 ps. Figure 2c plots the magnetic-field dependence of ω_L and T_2^* obtained by fitting all of the TRFR traces in Figure 2a (see Figure S8 for fits). The magnitude of ω_L increases linearly with increasing B_T. Fitting this trend yields |g| = 0.88, which matches the g-value obtained through FFT of these data (|g| = 0.86, Figure 2b, inset; and Figure S7). Based on first-principles models of metal-halide perovskite magneto-optics,[38,39] we assign the measured species as precessing holes. The g-value from Figure 2c agrees well with the hole g-value reported for bulk $CsPbBr_3$ (|g| = 0.76),[8] supporting this assignment. It also falls within the range of reported $CsPbBr_3$ nanocrystal hole g-values (Table S1).[39,40] FFT traces additionally show a weak, broad shoulder at |g| ~ 2 (see Figure S9) that coincides with the electron g-value of ~2 reported for bulk and nanocrystalline $CsPbBr_3$.[8,39,40] Although distinct, this signal is too weak to be thoroughly analyzed with confidence. The lack of a long-lived TRFR signal attributable to photogenerated electrons likely reflects rapid dephasing. Although rapid electron trapping[41] could conceivably be responsible, the short PL decay times combined with the near-unity PLQYs (*vide infra*) under these conditions suggest that electron spin dynamics in these nanocrystals are not dominated by trapping. We note that trapped carriers do not generate large band-edge TRFR signals.

It can be challenging to distinguish between excitons and trions because of their similar decay times at low temperatures.[40] Positive trions would show no hole precession and are therefore incompatible with the data. If negative trions dominated the TRFR signals, then only unpaired holes would be observed, but instead we also observe a distinct electron TRFR signal ($g_e \sim 2$, Figure S9). These considerations, combined with the nearly 100% PLQY at this temperature (*vide infra*), thus strongly suggest that the holes probed by TRFR here are associated with excitons. This conclusion is consistent with the very low pump and probe pulse fluences used here (see the SI) compared to those reportedly required for trion formation in $CsPbBr_3$ nanocrystals.[42]

At zero field, T_2^* is ~80 ps, but the application of a small magnetic field (0.13 T) increases T_2^* to 292 ± 12 ps. Notably, this latter value is essentially indistinguishable from the PL decay time of 312 ± 11 ps measured under the same conditions (Figure 2b). Above 0.13 T, T_2^* decreases monotonically with increasing B_T, as commonly observed in the TRFR of other semiconductors.[36] The decrease in T_2^* with increasing B_T is attributable to a distribution in g-values (Δg), for example, from a distribution in nanocrystal sizes or defect structures, and can be evaluated by fitting the T_2^* data with eq 2.[36]

$$1/T_2^* = 1/T_2 + 1/T_2^{inh} \approx 1/T_2 + \Delta g \mu_B B_T/\hbar \tag{2}$$

Here, $1/T_2^{inh}$ represents the sum of all inhomogeneous contributions to the ensemble spin-dephasing rate. This analysis yields Δg = 0.07 (~8%). The observation that Δg here is similar to that in bulk lead-halide perovskites[7,8] suggests that g-value heterogeneity stemming from the presence of different noncubic crystal structures and nanocrystal orientations is not the dominant contributor to T_2^*. The observation that T_2^* approaches but does not exceed the excitonic PL decay time further supports the conclusion that the holes probed by TRFR here are associated with excitons.

Short radiative lifetimes at low temperature are a distinctive characteristic of $CsPbBr_3$ and related lead-halide perovskite nanocrystals, whose lowest excitonic excited states are optically bright. This unique electronic structure enables the high $T_{2,o}/2\tau_{PL}$ ratios found for $CsPbBr_3$ nanocrystals.[14,16] Significantly, Figure 2 shows that T_2^* is similar to τ_{PL}, indicating that photogenerated hole spins retain their transverse coherence throughout a large portion of the excited-state lifetime. Consequently, a large fraction of the luminescence involves coherent polarized hole spins. Moreover, this fraction can be tuned using a magnetic field. For example, T_2^*/τ_{PL} at zero field indicates that ∼26% of emitted photons involve coherent hole spins, but increasing B_T to 0.13 T raises this value to ∼95% (see Figure S4). The near equivalence of T_2^* and τ_{PL} at 0.13 T indicates that even inhomogeneous hole transverse spin-dephasing times in $CsPbBr_3$ nanocrystals are primarily limited by recombination and, hence, that the hole T_2 in, e.g., $CsPbBr_3$ nanocrystal single-photon emitters is entirely population limited.

To investigate the origins of hole spin dephasing in $CsPbBr_3$ nanocrystals, we explored the PL temperature dependence. Figure 3a shows a color map of nanocrystal PL intensities measured from 4.5 to 300 K. As the temperature is increased from 4.5 K, the near-band-edge PL peak broadens and shows an anti-Varshni blue-shift characteristic of $CsPbBr_3$,[43] while decreasing in intensity. Figure 3b plots the integrated PL intensity ($I(T)$) and PL full-width-at-half-maximum (fwhm, $\Gamma(T)$) vs temperature. $I(T)$ is constant between 4.5 and ∼100 K but decreases rapidly above 100 K. These data, in conjunction with the PLQY of ∼30% at room temperature under these conditions, suggest that the PLQY between 4.5 and 100 K is close to 100%, as observed previously.[16,44] We interpret the temperature dependence in Figure 3b as thermally assisted exciton dissociation. In this scenario, the exciton-binding energy (E_B) can be estimated by fitting $I(T)$ with eq 3, where I_0 is the PL intensity at 0 K, A is a prefactor, and k_B is the Boltzmann constant.

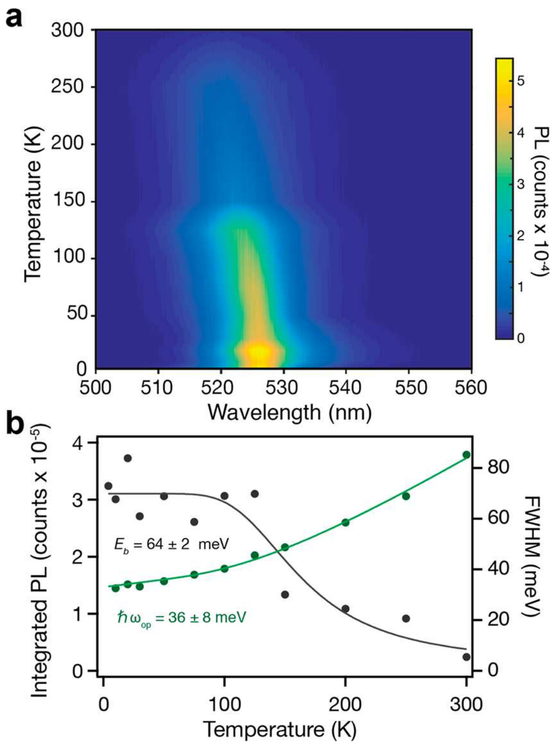

Figure 3. (a) Variable-temperature PL intensities for the $CsPbBr_3$/ZFP3 film used to collect TRFR data, measured using 375 nm excitation. (b) Integrated exciton PL intensity (I(T), black) and fwhm ($\Gamma(T)$, green) plotted vs temperature. The solid curves show fits of the data using eqs 3 and 4. Fitting the variable-temperature PL intensities yields an exciton binding energy of E_B = 64 ± 2 meV. Fitting the exciton fwhm data yields an optical phonon energy of $\hbar\omega_{op}$ = 36 ± 8 meV.

$$I(T) = \frac{I_0}{1 + Ae^{-E_B/k_BT}} \tag{3}$$

This analysis yields E_B = 64 ± 2 meV, similar to previous reports, as well as A = 85 and $I_0 = 3.05 \times 10^5$ counts.[29,30] In addition, $\Gamma(T)$ can be analyzed by fitting the data in Figure 3b with an independent Boson model described using eq 4, where Γ_0, σ, and Γ_{op} reflect inhomogeneous PL broadening, an acoustic phonon contribution, and exciton-optical phonon coupling with energy $\hbar\omega_{op}$, respectively.[45]

$$\Gamma(T) = \Gamma_0 + \sigma T + \frac{\Gamma_{op}}{e^{-\hbar\omega_{op}/k_BT} - 1} \tag{4}$$

This analysis reveals exciton coupling to longitudinal optical (LO) phonons with energy $\hbar\omega_{op}$ = 36 ± 8 meV, as well as Γ_0 = 32 ± 1 meV, σ = 60 ± 20 μeV, and Γ_{op} = 80 ± 12 meV, consistent with other perovskite nanocrystal reports (Table S4).[30,46,47]

Figure 4 plots T_2^* vs temperature for data measured with and without a transverse magnetic field of 0.60 T. Three distinct regimes are identified in the temperature dependence of T_2^*. Below 50 K, T_2^* is much larger in the transverse field than at zero-field. For example, at 4.5 K, T_2^* is ∼170 ps when B_T =

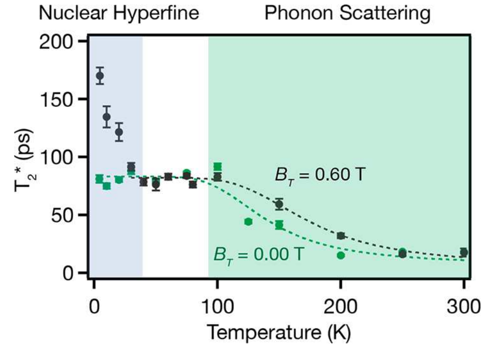

Figure 4. Ensemble inhomogeneous transverse spin-dephasing times (T_2^*) measured for $CsPbBr_3$ nanocrystals with and without an applied magnetic field, plotted as a function of sample temperature. The blue area highlights the regime where other dephasing mechanisms are frozen out, and the applied magnetic field boosts T_2^* by suppressing inhomogeneous hyperfine fields. The green area emphasizes the regime where thermally activated phonon scattering dominates spin dephasing. The dashed green curve shows a fit to eq 5 of the entire zero-field T_2^* data set. The dashed black curve shows a fit to eq 5 of the T_2^* data collected at 0.60 T between 40 and 300 K. See Figure S5 for time traces.

0.60 T but only ~80 ps when B_T = 0 T (see Figure S6). Whereas the zero-field T_2^* is independent of temperature in this regime, T_2^* measured at 0.60 T decreases rapidly with increasing temperature until the two data sets converge at ~50 K. Between 50 and 100 K, T_2^* is independent of both temperature and applied field. Above ~100 K, both data sets show T_2^* decreasing with increasing temperature, dropping to ~16 ps at room temperature.

These observations suggest two dominant thermally activated spin-dephasing mechanisms in this material: a field-dependent mechanism active at low temperatures and a field-independent mechanism active at higher temperatures. We attribute the large increase in T_2^* upon application of the transverse magnetic field below 50 K to field-induced suppression of local magnetic-field inhomogeneities due to nuclear hyperfine interactions that accelerate dephasing.[20,33,48−50] The highly ionic nature of the metal-halide perovskite lattice and the large Pb 6s contribution to the carrier wave function at the valence-band edge favor strong Fermi-contact hyperfine coupling (Table S2).[50−52] Accumulation of Pb^{2+} nuclear spin polarization may further exacerbate the effect of inhomogeneous nuclear magnetic fields.[8] Applied magnetic fields can also reduce dephasing caused by spontaneous electromagnetic fields generated by the Rashba effect, as observed in III−V nanomaterials.[53,54]

The higher-temperature (100−300 K) dephasing is attributed to coupling between photogenerated spins and LO phonons. For example, at elevated temperatures and small B_T, elastic scattering of phonons can modulate the hyperfine field, causing decoherence.[55,56] Similarly, the Elliott−Yafet mechanism[9,57] involves spin-flip processes driven by phonon coupling, and the Dyakonov−Perel mechanism[58] involves inhomogeneous magnetic fields due to noncentrosymmetric local distortions, potentially driven by optical phonons in this case.[12,59] The effect of phonon-modulated hyperfine fields on dephasing can be described by eq 5, where the phonon-induced decoherence term, Λ, is a function of the nuclear spin values, their concentration, the volume of the nanocrystal, and the hyperfine coupling strength. $T_2^*(0)$ represents the low-temperature T_2^* at zero magnetic field, and $F(x) = (1-\tanh^2(x))\tanh(x)$.

$$T_2^*(T) = \left(1/T_2^*(0) + \Lambda F\left(\frac{\hbar\omega}{k_B T}\right)\right)^{-1} \tag{5}$$

This fitting yields $\hbar\omega = 29 \pm 5$ meV ($\Lambda = 0.27$ ps^{-1}) for the zero-field data and $\hbar\omega = 36 \pm 5$ meV ($\Lambda = 0.32$ ps^{-1}) for the 0.60 T data, which are within experimental uncertainty of one another. Both are similar to the LO phonon frequency that dominates exciton−phonon coupling ($\hbar\omega = 36 \pm 8$ meV, Figure 3b). Exciton coupling with acoustic phonons is weak in $CsPbBr_3$ nanocrystals at low temperature,[43] which could explain its limited influence on spin dephasing in this temperature range. Thermally activated spin dephasing in other lead-halide perovskites has been described as Arrhenius-like and attributed to LO phonons with a temperature dependence similar to eq 5.[7−9]

Although the temperature dependence of T_2^* in these $CsPbBr_3$ nanocrystals at zero field is qualitatively similar to that measured for bulk metal-halide perovskites, including $CsPbBr_3$ single crystals,[7,8] the data here reveal several important contrasts between spins in nanocrystalline and bulk $CsPbBr_3$. Most notably, the photogenerated spins monitored by TRFR in bulk $CsPbBr_3$ reportedly[8,32] accumulate over time, likely because of deep carrier trapping, such that they cannot be directly associated with the emissive excited state of the material. This conclusion is supported by the very low PLQYs and by T_2^* values that exceed the PL decay time in these bulk samples.[29] Bulk samples also showed sizable variations in hole T_2^* depending on excitation position, with values ranging from 0.7 to 1.9 ns.[8] In contrast, because of the combination of short radiative lifetimes and high PLQYs (~100% at 4.5 K) in the nanocrystals, the spins of photogenerated holes in $CsPbBr_3$ nanocrystals *are* associated with the luminescent excited state and appear to remain coherent for the entire lifetime of this excited state when under a small magnetic field, i.e., until they recombine radiatively. Consistent with these observations, there is also essentially no variation in T_2^* at different excitation positions within a given nanocrystal film or between nanocrystal samples (see Table S3 and Figure S3).

A second notable contrast is that T_2^* shows a strong field dependence at low temperatures in the $CsPbBr_3$ nanocrystals (~300% increase from B_T = 0 to 0.13 T, Figures 2c and 4), but it does not show a comparably strong field dependence in bulk $CsPbBr_3$ (~20% increase from B_T = 0 to 0.125 T).[8] This contrast may stem from confinement-enhanced hyperfine coupling in the nanocrystals.[24,33,48,59−61] In this scenario, inhomogeneous hyperfine fields reduce T_2^* more in nanocrystalline $CsPbBr_3$ than in bulk, and conversely, their suppression by magnetic fields has a greater impact on T_2^* in the nanocrystals. We note that carrier spins within nanocrystals are also subject to hyperfine interactions with the surrounding nuclear spin bath, e.g., from proton-bearing surface ligands, solvent, or polymer matrices,[62] distinguishing nanocrystals from bulk. Although T_2^* is not necessarily related to optical coherence ($T_{2,o}$), it is intriguing that optical dephasing[16] and spin dephasing both occur with similar time constants of 50−80 ps in $CsPbBr_3$ nanocrystals at zero field. In other promising single-photon emitters like III−V nanocrystals, optical coherence is limited by nuclear-spin-flip dynamics.[63−65] If $CsPbBr_3$ nanocrystal optical coherence is similarly limited by spin-flip processes and carrier interactions with the nuclear spin bath, small magnetic fields may extend these optical coherence times, just as they extend the spin coherence times here (Figures 2c and 4).

Finally, it is noteworthy that spin coherences are preserved at much higher temperatures in $CsPbBr_3$ nanocrystals than in bulk. Although the benefits of a magnetic field are restricted to temperatures below ~50 K, T_2^* values of 80 ps at 100 K and 16 ps at room temperature are still observed in the nanocrystals. In comparison, T_2^* in bulk $CsPbBr_3$ decreases precipitously above 20 K, dropping to ~20 ps at 100 K, above which it could not be measured.[8] $CsPbBr_3$ nanocrystals thus present greater opportunity for measurement and application at elevated temperatures. Furthermore, the different spin dephasing mechanisms active at various temperatures suggest potential strategies to engineer spin properties in metal-halide nanocrystals. For example, tuning or alloying the B-site cation[66,67] to modify the hyperfine interactions may influence the hole T_2^* at low temperature or introduce new exchange contributions to the *g*-value. Similarly, modifying nanocrystal phonon energies through ion exchange, pressure, or shape control may allow extension of spin applications to elevated temperatures.

In summary, carrier spin-dephasing dynamics in metal-halide perovskite nanocrystals have been measured for the first time. Using TRFR spectroscopy, coherent spin precession of photogenerated holes in $CsPbBr_3$ nanocrystals has been observed from cryogenic temperatures up to room temperature. At low temperatures, spin coherence is limited by inhomogeneous hyperfine fields, but the spin-dephasing time can be extended dramatically by application of a small magnetic field. Under these conditions, T_2^* approaches τ_{PL}, and ~95% of emitted photons derive from excitons with coherent spin-polarized holes. Variable-temperature TRFR and PL measurements are consistent with additional spin dephasing at elevated temperatures driven by thermally activated LO phonons. The data highlight several major contrasts between spins in bulk and nanocrystalline $CsPbBr_3$. Overall, these results advance our fundamental understanding of spin dephasing in lead-halide perovskites and provide a basis for engineering such spin properties chemically or with magnetic fields, potentially opening the door to enticing spintronic and quantum information applications.

■ ASSOCIATED CONTENT

Supporting Information

The Supporting Information is available free of charge at https://pubs.acs.org/doi/10.1021/acs.nanolett.0c03329.

> Additional details about nanocrystal synthesis and variable-temperature PL lifetimes, TRFR traces used in Figures 2 and 4 as well as TRFR traces from replicate samples, and FFTs of TRFR traces (PDF)

■ AUTHOR INFORMATION

Corresponding Author

Daniel R. Gamelin − *Department of Chemistry and Molecular Engineering & Sciences Institute, University of Washington, Seattle, Washington 98195-1700, United States;* orcid.org/0000-0003-2888-9916; Email: gamelin@chem.washington.edu

Authors

Matthew J. Crane − *Department of Chemistry, University of Washington, Seattle, Washington 98195-1700, United States;* orcid.org/0000-0001-8461-4808

Laura M. Jacoby − *Department of Chemistry, University of Washington, Seattle, Washington 98195-1700, United States;* orcid.org/0000-0002-9308-7162

Theodore A. Cohen − *Department of Chemistry, Molecular Engineering & Sciences Institute, and Department of Materials Science & Engineering, University of Washington, Seattle, Washington 98195-1700, United States;* orcid.org/0000-0001-7170-3211

Yunping Huang − *Department of Materials Science & Engineering, University of Washington, Seattle, Washington 98195-2120, United States*

Christine K. Luscombe − *Department of Chemistry, Molecular Engineering & Sciences Institute, and Department of Materials Science & Engineering, University of Washington, Seattle, Washington 98195-1700, United States;* orcid.org/0000-0001-7456-1343

Complete contact information is available at: https://pubs.acs.org/10.1021/acs.nanolett.0c03329

Author Contributions

[‖]M.J.C. and L.M.J. contributed equally to this work.

Notes

The authors declare no competing financial interest.

■ ACKNOWLEDGMENTS

This research was supported by the National Science Foundation (NSF) through DMR-1807394 and through the UW Molecular Engineering Materials Center, a Materials Research Science and Engineering Center (DMR-1719797). M.J.C. acknowledges support from the Washington Research Foundation through a Postdoctoral Fellowship. L.M.J. and Y.H. acknowledge support from the Data Intensive Research Enabling Clean Technology (DIRECT) NSF National Research Traineeship (DGE-1633216). Part of this work was conducted at the Molecular Analysis Facility, a National Nanotechnology Coordinated Infrastructure site at the University of Washington that is supported in part by the National Science Foundation (ECC-1542101), the University of Washington, the UW Molecular Engineering & Sciences Institute, and the UW Clean Energy Institute. The authors thank Prof. Devin Mackenzie for thoughtful input and support.

■ REFERENCES

(1) Stoumpos, C. C.; Kanatzidis, M. G. The Renaissance of Halide Perovskites and Their Evolution as Emerging Semiconductors. *Acc. Chem. Res.* **2015**, *48*, 2791−2802.

(2) Stranks, S. D.; Snaith, H. J. Metal-halide perovskites for photovoltaic and light-emitting devices. *Nat. Nanotechnol.* **2015**, *10*, 391−402.

(3) Protesescu, L.; Yakunin, S.; Bodnarchuk, M. I.; Krieg, F.; Caputo, R.; Hendon, C. H.; Yang, R. X.; Walsh, A.; Kovalenko, M. V. Nanocrystals of Cesium Lead Halide Perovskites ($CsPbX_3$, X = Cl, Br, and I): Novel Optoelectronic Materials Showing Bright Emission with Wide Color Gamut. *Nano Lett.* **2015**, *15*, 3692−3696.

(4) Seo, J.; Noh, J. H.; Seok, S. I. Rational Strategies for Efficient Perovskite Solar Cells. *Acc. Chem. Res.* **2016**, *49*, 562−572.

(5) Docampo, P.; Bein, T. A Long-Term View on Perovskite Optoelectronics. *Acc. Chem. Res.* **2016**, *49*, 339−346.

(6) Huang, H.; Bodnarchuk, M. I.; Kershaw, S. V.; Kovalenko, M. V.; Rogach, A. L. Lead Halide Perovskite Nanocrystals in the Research Spotlight: Stability and Defect Tolerance. *ACS Energy Lett.* **2017**, *2*, 2071−2083.

(7) Odenthal, P.; Talmadge, W.; Gundlach, N.; Wang, R.; Zhang, C.; Sun, D.; Yu, Z.-G.; Valy Vardeny, Z.; Li, Y. S. Spin-polarized exciton quantum beating in hybrid organic−inorganic perovskites. *Nat. Phys.* **2017**, *13*, 894−899.

(8) Belykh, V. V.; Yakovlev, D. R.; Glazov, M. M.; Grigoryev, P. S.; Hussain, M.; Rautert, J.; Dirin, D. N.; Kovalenko, M. V.; Bayer, M. Coherent spin dynamics of electrons and holes in CsPbBr 3 perovskite crystals. *Nat. Commun.* **2019**, *10*, 673.

(9) Strohmair, S.; Dey, A.; Tong, Y.; Polavarapu, L.; Bohn, B. J.; Feldmann, J. Spin Polarization Dynamics of Free Charge Carriers in $CsPbI_3$ Nanocrystals. *Nano Lett.* **2020**, *20*, 4724−4730.

(10) Giovanni, D.; Ma, H.; Chua, J.; Grätzel, M.; Ramesh, R.; Mhaisalkar, S.; Mathews, N.; Sum, T. C. Highly Spin-Polarized Carrier Dynamics and Ultralarge Photoinduced Magnetization in $CH_3NH_3PbI_3$ Perovskite Thin Films. *Nano Lett.* **2015**, *15*, 1553−1558.

(11) Li, Y.; Luo, X.; Liu, Y.; Lu, X.; Wu, K. Size- and Composition-Dependent Exciton Spin Relaxation in Lead Halide Perovskite Quantum Dots. *ACS Energy Lett.* **2020**, *5*, 1701−1708.

(12) Isarov, M.; Tan, L. Z.; Bodnarchuk, M. I.; Kovalenko, M. V.; Rappe, A. M.; Lifshitz, E. Rashba Effect in a Single Colloidal $CsPbBr_3$ Perovskite Nanocrystal Detected by Magneto-Optical Measurements. *Nano Lett.* **2017**, *17*, 5020−5026.

(13) Kepenekian, M.; Even, J. Rashba and Dresselhaus Couplings in Halide Perovskites: Accomplishments and Opportunities for Spintronics and Spin−Orbitronics. *J. Phys. Chem. Lett.* **2017**, *8*, 3362−3370.

(14) Becker, M. A.; Vaxenburg, R.; Nedelcu, G.; Sercel, P. C.; Shabaev, A.; Mehl, M. J.; Michopoulos, J. G.; Lambrakos, S. G.;

Bernstein, N.; Lyons, J. L.; Stöferle, T.; Mahrt, R. F.; Kovalenko, M. V.; Norris, D. J.; Rainò, G.; Efros, A. L. Bright triplet excitons in caesium lead halide perovskites. *Nature* **2018**, *553*, 189−193.

(15) Becker, M. A.; Scarpelli, L.; Nedelcu, G.; Rainò, G.; Masia, F.; Borri, P.; Stöferle, T.; Kovalenko, M. V.; Langbein, W.; Mahrt, R. F. Long Exciton Dephasing Time and Coherent Phonon Coupling in $CsPbBr_2Cl$ Perovskite Nanocrystals. *Nano Lett.* **2018**, *18*, 7546−7551.

(16) Utzat, H.; Sun, W.; Kaplan, A. E. K.; Krieg, F.; Ginterseder, M.; Spokoyny, B.; Klein, N. D.; Shulenberger, K. E.; Perkinson, C. F.; Kovalenko, M. V.; Bawendi, M. G. Coherent single-photon emission from colloidal lead halide perovskite quantum dots. *Science* **2019**, *363*, 1068−1072.

(17) Berezovsky, J.; Gywat, O.; Meier, F.; Battaglia, D.; Peng, X.; Awschalom, D. D. Initialization and read-out of spins in coupled core−shell quantum dots. *Nat. Phys.* **2006**, *2*, 831−834.

(18) Utzat, H.; Shulenberger, K. E.; Achorn, O. B.; Nasilowski, M.; Sinclair, T. S.; Bawendi, M. G. Probing Linewidths and Biexciton Quantum Yields of Single Cesium Lead Halide Nanocrystals in Solution. *Nano Lett.* **2017**, *17*, 6838−6846.

(19) Wang, J.; Zhang, C.; Liu, H.; McLaughlin, R.; Zhai, Y.; Vardeny, S. R.; Liu, X.; McGill, S.; Semenov, D.; Guo, H.; Tsuchikawa, R.; Deshpande, V. V.; Sun, D.; Vardeny, Z. V. Spin-optoelectronic devices based on hybrid organic-inorganic trihalide perovskites. *Nat. Commun.* **2019**, *10*, 129.

(20) Balasubramanian, G.; Neumann, P.; Twitchen, D.; Markham, M.; Kolesov, R.; Mizuochi, N.; Isoya, J.; Achard, J.; Beck, J.; Tissler, J.; Jacques, V.; Hemmer, P. R.; Jelezko, F.; Wrachtrup, J. Ultralong spin coherence time in isotopically engineered diamond. *Nat. Mater.* **2009**, *8*, 383−387.

(21) Crane, M. J.; Petrone, A.; Beck, R. A.; Lim, M. B.; Zhou, X.; Li, X.; Stroud, R. M.; Pauzauskie, P. J. High-pressure, high-temperature molecular doping of nanodiamond. *Sci. Adv.* **2019**, *5*, No. eaau6073.

(22) Santori, C.; Fattal, D.; Vučković, J.; Solomon, G. S.; Yamamoto, Y. Indistinguishable photons from a single-photon device. *Nature* **2002**, *419*, 594−597.

(23) Gottscholl, A.; Kianinia, M.; Soltamov, V.; Orlinskii, S.; Mamin, G.; Bradac, C.; Kasper, C.; Krambrock, K.; Sperlich, A.; Toth, M.; Aharonovich, I.; Dyakonov, V. Initialization and read-out of intrinsic spin defects in a van der Waals crystal at room temperature. *Nat. Mater.* **2020**, *19*, 540−545.

(24) Petta, J. R.; Johnson, A. C.; Taylor, J. M.; Laird, E. A.; Yacoby, A.; Lukin, M. D.; Marcus, C. M.; Hanson, M. P.; Gossard, A. C. Coherent Manipulation of Coupled Electron Spins in Semiconductor Quantum Dots. *Science* **2005**, *309*, 2180−2184.

(25) Yao, W.; Liu, R.-B.; Sham, L. J. Theory of Control of the Spin-Photon Interface for Quantum Networks. *Phys. Rev. Lett.* **2005**, *95*, 030504.

(26) van Loock, P.; Ladd, T. D.; Sanaka, K.; Yamaguchi, F.; Nemoto, K.; Munro, W. J.; Yamamoto, Y. Hybrid Quantum Repeater Using Bright Coherent Light. *Phys. Rev. Lett.* **2006**, *96*, 240501.

(27) De Greve, K.; Yu, L.; McMahon, P. L.; Pelc, J. S.; Natarajan, C. M.; Kim, N. Y.; Abe, E.; Maier, S.; Schneider, C.; Kamp, M.; Höfling, S.; Hadfield, R. H.; Forchel, A.; Fejer, M. M.; Yamamoto, Y. Quantum-dot spin−photon entanglement via frequency down-conversion to telecom wavelength. *Nature* **2012**, *491*, 421−425.

(28) Wang, T.-J.; Song, S.-Y.; Long, G. L. Quantum repeater based on spatial entanglement of photons and quantum-dot spins in optical microcavities. *Phys. Rev. A: At., Mol., Opt. Phys.* **2012**, *85*, 062311.

(29) Ling, Y.; Tan, L.; Wang, X.; Zhou, Y.; Xin, Y.; Ma, B.; Hanson, K.; Gao, H. Composite Perovskites of Cesium Lead Bromide for Optimized Photoluminescence. *J. Phys. Chem. Lett.* **2017**, *8*, 3266−3271.

(30) Shinde, A.; Gahlaut, R.; Mahamuni, S. Low-Temperature Photoluminescence Studies of $CsPbBr_3$ Quantum Dots. *J. Phys. Chem. C* **2017**, *121*, 14872−14878.

(31) Sercel, P. C.; Lyons, J. L.; Wickramaratne, D.; Vaxenburg, R.; Bernstein, N.; Efros, A. L. Exciton Fine Structure in Perovskite Nanocrystals. *Nano Lett.* **2019**, *19*, 4068−4077.

(32) Feng, D.; Yakovlev, D. R.; Dubertret, B.; Bayer, M. Charge Separation Dynamics in CdSe/CdS Core/Shell Nanoplatelets Addressed by Coherent Electron Spin Precession. *ACS Nano* **2020**, *14*, 7237−7244.

(33) Whitaker, K. M.; Ochsenbein, S. T.; Smith, A. L.; Echodu, D. C.; Robinson, B. H.; Gamelin, D. R. Hyperfine Coupling in Colloidal n-Type ZnO Quantum Dots: Effects on Electron Spin Relaxation. *J. Phys. Chem. C* **2010**, *114*, 14467−14472.

(34) Crooker, S. A.; Awschalom, D. D.; Samarth, N. Time-resolved Faraday rotation spectroscopy of spin dynamics in digital magnetic heterostructures. *IEEE J. Sel. Top. Quantum Electron.* **1995**, *1*, 1082−1092.

(35) Awschalom, D. D.; Kikkawa, J. M. Electron Spin and Optical Coherence in Semiconductors. *Phys. Today* **1999**, *52*, 33.

(36) Yakovlev, D. R.; Bayer, M. Coherent Spin Dynamics of Carriers. In *Spin Physics in Semiconductors*; Dyakonov, M. I., Ed.; Springer: Berlin, Heidelberg, 2008; pp 135−177.

(37) Cohen, T. A.; Huang, Y.; Bricker, N. A.; Juhl, C. S.; Milstein, T. J.; MacKenzie, J. D.; Luscombe, C. K.; Gamelin, D. R. Modular Zwitterion-Functionalized Poly(Isopropyl Methacrylate) Polymers for Hosting Luminescent Lead-Halide Perovskite Nanocrystals. 2020, submitted.

(38) Yu, Z. G. Effective-mass model and magneto-optical properties in hybrid perovskites. *Sci. Rep.* **2016**, *6*, 28576.

(39) Canneson, D.; Shornikova, E. V.; Yakovlev, D. R.; Rogge, T.; Mitioglu, A. A.; Ballottin, M. V.; Christianen, P. C. M.; Lhuillier, E.; Bayer, M.; Biadala, L. Negatively Charged and Dark Excitons in $CsPbBr_3$ Perovskite Nanocrystals Revealed by High Magnetic Fields. *Nano Lett.* **2017**, *17*, 6177−6183.

(40) Fu, M.; Tamarat, P.; Huang, H.; Even, J.; Rogach, A. L.; Lounis, B. Neutral and Charged Exciton Fine Structure in Single Lead Halide Perovskite Nanocrystals Revealed by Magneto-optical Spectroscopy. *Nano Lett.* **2017**, *17*, 2895−2901.

(41) Nenon, D. P.; Pressler, K.; Kang, J.; Koscher, B. A.; Olshansky, J. H.; Osowiecki, W. T.; Koc, M. A.; Wang, L.-W.; Alivisatos, A. P. Design Principles for Trap-Free $CsPbX_3$ Nanocrystals: Enumerating and Eliminating Surface Halide Vacancies with Softer Lewis Bases. *J. Am. Chem. Soc.* **2018**, *140*, 17760−17772.

(42) Nakahara, S.; Tahara, H.; Yumoto, G.; Kawawaki, T.; Saruyama, M.; Sato, R.; Teranishi, T.; Kanemitsu, Y. Suppression of Trion Formation in $CsPbBr_3$ Perovskite Nanocrystals by Postsynthetic Surface Modification. *J. Phys. Chem. C* **2018**, *122*, 22188−22193.

(43) Saran, R.; Heuer-Jungemann, A.; Kanaras, A. G.; Curry, R. J. Giant Bandgap Renormalization and Exciton−Phonon Scattering in Perovskite Nanocrystals. *Adv. Opt. Mater.* **2017**, *5*, 1700231.

(44) Zheng, X.; Yuan, S.; Liu, J.; Yin, J.; Yuan, F.; Shen, W.-S.; Yao, K.; Wei, M.; Zhou, C.; Song, K.; Zhang, B.-B.; Lin, Y.; Hedhili, M. N.; Wehbe, N.; Han, Y.; Sun, H.-T.; Lu, Z.-H.; Anthopoulos, T. D.; Mohammed, O. F.; Sargent, E. H.; Liao, L.-S.; Bakr, O. M. Chlorine Vacancy Passivation in Mixed Halide Perovskite Quantum Dots by Organic Pseudohalides Enables Efficient Rec. 2020 Blue Light-Emitting Diodes. *ACS Energy Lett.* **2020**, *5*, 793−798.

(45) Rudin, S.; Reinecke, T. L. Temperature-dependent exciton linewidths in semiconductor quantum wells. *Phys. Rev. B: Condens. Matter Mater. Phys.* **1990**, *41*, 3017−3027.

(46) Zhang, F.; Zhong, H.; Chen, C.; Wu, X.-g.; Hu, X.; Huang, H.; Han, J.; Zou, B.; Dong, Y. Brightly Luminescent and Color-Tunable Colloidal $CH_3NH_3PbX_3$ (X = Br, I, Cl) Quantum Dots: Potential Alternatives for Display Technology. *ACS Nano* **2015**, *9*, 4533−4542.

(47) Shi, Z.; Li, Y.; Zhang, Y.; Chen, Y.; Li, X.; Wu, D.; Xu, T.; Shan, C.; Du, G. High-Efficiency and Air-Stable Perovskite Quantum Dots Light-Emitting Diodes with an All-Inorganic Heterostructure. *Nano Lett.* **2017**, *17*, 313−321.

(48) Merkulov, I. A.; Efros, A. L.; Rosen, M. Electron spin relaxation by nuclei in semiconductor quantum dots. *Phys. Rev. B: Condens. Matter Mater. Phys.* **2002**, *65*, 205309.

(49) Feng, D. H.; Li, X.; Jia, T. Q.; Pan, X. Q.; Sun, Z. R.; Xu, Z. Z. Long-lived, room-temperature electron spin coherence in colloidal CdS quantum dots. *Appl. Phys. Lett.* **2012**, *100*, 122406.

(50) Chekhovich, E. A.; Glazov, M. M.; Krysa, A. B.; Hopkinson, M.; Senellart, P.; Lemaître, A.; Skolnick, M. S.; Tartakovskii, A. I. Element-sensitive measurement of the hole−nuclear spin interaction in quantum dots. *Nat. Phys.* **2013**, *9*, 74−78.

(51) Fischer, J.; Coish, W. A.; Bulaev, D. V.; Loss, D. Spin decoherence of a heavy hole coupled to nuclear spins in a quantum dot. *Phys. Rev. B: Condens. Matter Mater. Phys.* **2008**, *78*, 155329.

(52) Syperek, M.; Yakovlev, D. R.; Yugova, I. A.; Misiewicz, J.; Sedova, I. V.; Sorokin, S. V.; Toropov, A. A.; Ivanov, S. V.; Bayer, M. Long-lived electron spin coherence in CdSe/Zn(S,Se) self-assembled quantum dots. *Phys. Rev. B: Condens. Matter Mater. Phys.* **2011**, *84*, 085304.

(53) Beschoten, B.; Johnston-Halperin, E.; Young, D. K.; Poggio, M.; Grimaldi, J. E.; Keller, S.; DenBaars, S. P.; Mishra, U. K.; Hu, E. L.; Awschalom, D. D. Spin coherence and dephasing in GaN. *Phys. Rev. B: Condens. Matter Mater. Phys.* **2001**, *63*, 121202.

(54) Weng, M. Q.; Wu, M. W. Rashba-effect-induced spin dephasing in n-type InAs quantum wells. *J. Phys.: Condens. Matter* **2003**, *15*, 5563−5576.

(55) Semenov, Y. G.; Kim, K. W. Elastic spin-relaxation processes in semiconductor quantum dots. *Phys. Rev. B: Condens. Matter Mater. Phys.* **2007**, *75*, 195342.

(56) Hernandez, F. G. G.; Greilich, A.; Brito, F.; Wiemann, M.; Yakovlev, D. R.; Reuter, D.; Wieck, A. D.; Bayer, M. Temperature-induced spin-coherence dissipation in quantum dots. *Phys. Rev. B: Condens. Matter Mater. Phys.* **2008**, *78*, 041303.

(57) Baral, A.; Vollmar, S.; Kaltenborn, S.; Schneider, H. C. Re-examination of the Elliott−Yafet spin-relaxation mechanism. *New J. Phys.* **2016**, *18*, 023012.

(58) Wu, M. W.; Ning, C. Z. Dyakonov-Perel Effect on Spin Dephasing in n-Type GaAs. *Phys. Status Solidi B* **2000**, *222*, 523−534.

(59) Dyakonov, M. I. Basics of Semiconductor and Spin Physics. In *Spin Physics in Semiconductors*; Dyakonov, M. I., Ed. Springer: Berlin, Heidelberg, 2008; pp 1−28.

(60) Bloembergen, N. Nuclear magnetic relaxation in semiconductors. *Physica* **1954**, *20*, 1130−1133.

(61) Urbaszek, B.; Braun, P. F.; Amand, T.; Krebs, O.; Belhadj, T.; Lemaítre, A.; Voisin, P.; Marie, X. Efficient dynamical nuclear polarization in quantum dots: Temperature dependence. *Phys. Rev. B: Condens. Matter Mater. Phys.* **2007**, *76*, 201301.

(62) Schimpf, A. M.; Ochsenbein, S. T.; Gamelin, D. R. Surface Contributions to Mn^{2+} Spin Dynamics in Colloidal Doped Quantum Dots. *J. Phys. Chem. Lett.* **2015**, *6*, 457−463.

(63) Cywiński, Ł.; Witzel, W. M.; Das Sarma, S. Pure quantum dephasing of a solid-state electron spin qubit in a large nuclear spin bath coupled by long-range hyperfine-mediated interactions. *Phys. Rev. B: Condens. Matter Mater. Phys.* **2009**, *79*, 245314.

(64) Bluhm, H.; Foletti, S.; Neder, I.; Rudner, M.; Mahalu, D.; Umansky, V.; Yacoby, A. Dephasing time of GaAs electron-spin qubits coupled to a nuclear bath exceeding 200 μs. *Nat. Phys.* **2011**, *7*, 109−113.

(65) Accanto, N.; Masia, F.; Moreels, I.; Hens, Z.; Langbein, W.; Borri, P. Engineering the Spin−Flip Limited Exciton Dephasing in Colloidal CdSe/CdS Quantum Dots. *ACS Nano* **2012**, *6*, 5227−5233.

(66) Creutz, S. E.; Crites, E. N.; De Siena, M. C.; Gamelin, D. R. Colloidal Nanocrystals of Lead-Free Double-Perovskite (Elpasolite) Semiconductors: Synthesis and Anion Exchange To Access New Materials. *Nano Lett.* **2018**, *18*, 1118−1123.

(67) Bartel, C. J.; Sutton, C.; Goldsmith, B. R.; Ouyang, R.; Musgrave, C. B.; Ghiringhelli, L. M.; Scheffler, M. New tolerance factor to predict the stability of perovskite oxides and halides. *Sci. Adv.* **2019**, *5*, No. eaav0693.